Electronic Supplementary Information

Direct growth of nickel terephthalate on Ni foam with large mass-loading for high-performance supercapacitors

Qiulin Chen, Shuijin Lei*, Peiqin Deng, Xiuling Ou, Lianfu Chen, Wei Wang, Yanhe Xiao and Baochang Cheng

School of Materials Science and Engineering, Nanchang University, Nanchang, Jiangxi 330031, P. R. China

*To whom correspondence should be addressed. E-mail: shjlei@ncu.edu.cn

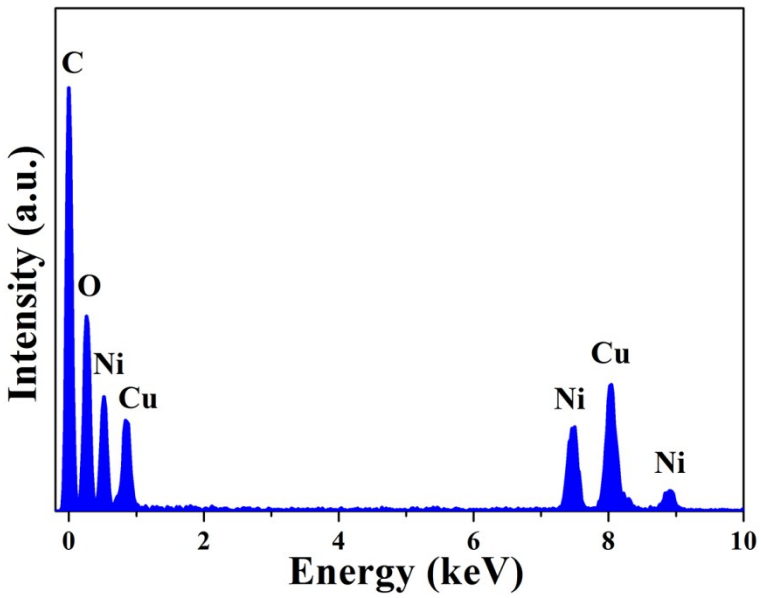

Fig. S1 EDS spectrum of the as-prepared Ni-Tp sample.

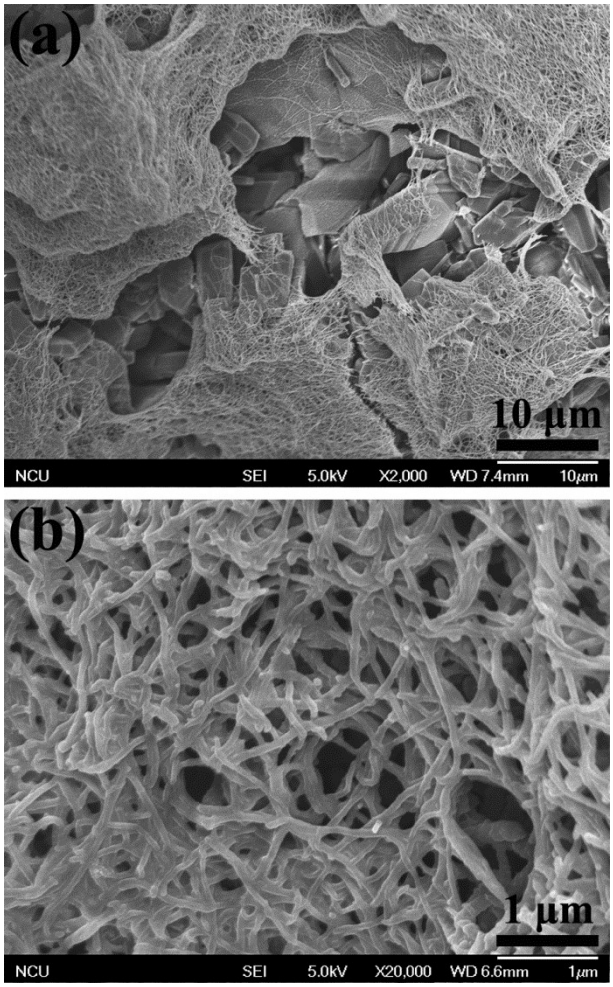

Fig. S2 (a) The high-magnification SEM image of the PANI coated Ni-Tp and (b) the close-up SEM image of the deposited PANI.

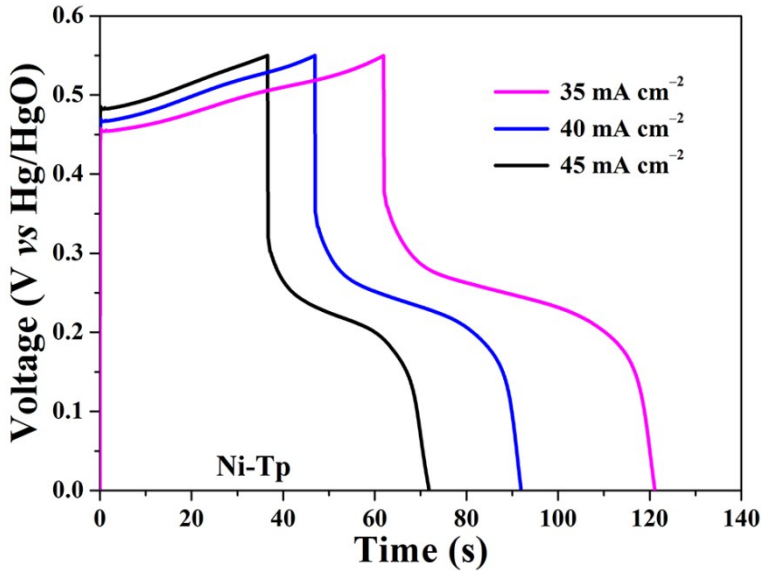

Fig. S3 GCD curves of the prepared Ni-Tp electrode at the current densities of 35, 40, and 45 mA cm^{-2}.

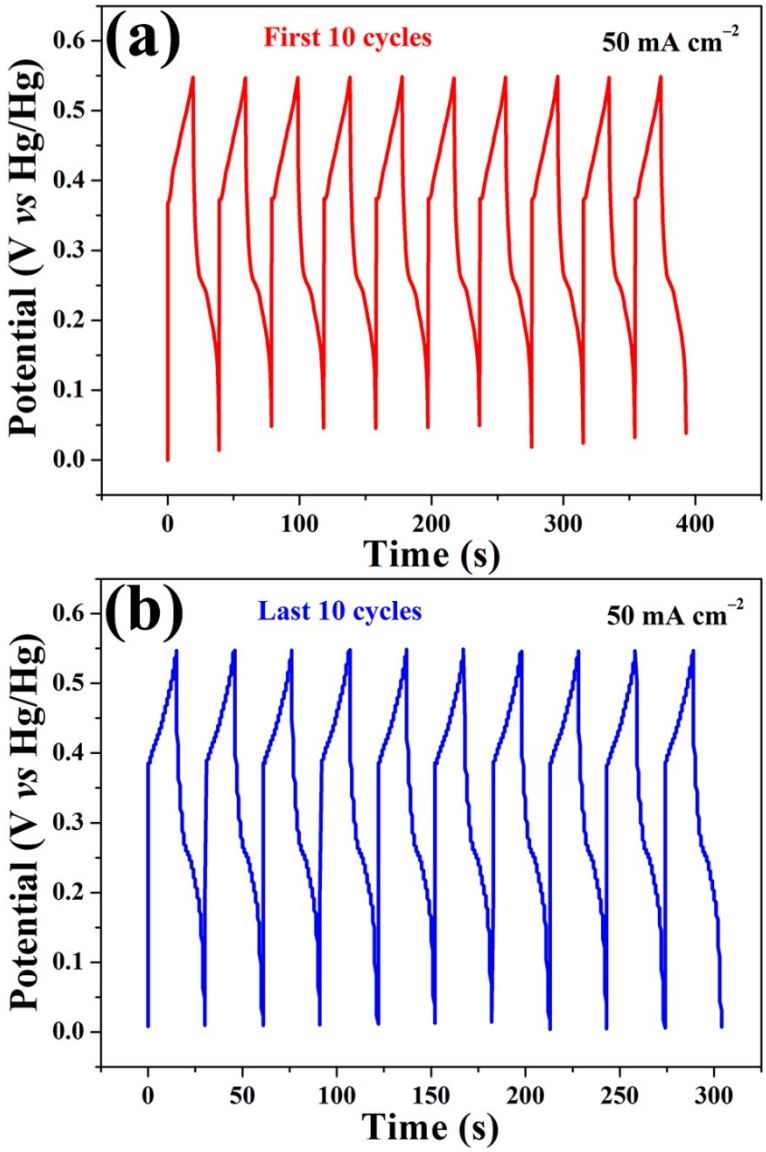

Fig. S4 The (a) first and (b) last ten charge-discharge cycles of the as-synthesized Ni-Tp electrode at a current density of 50 mA cm^{-2}.

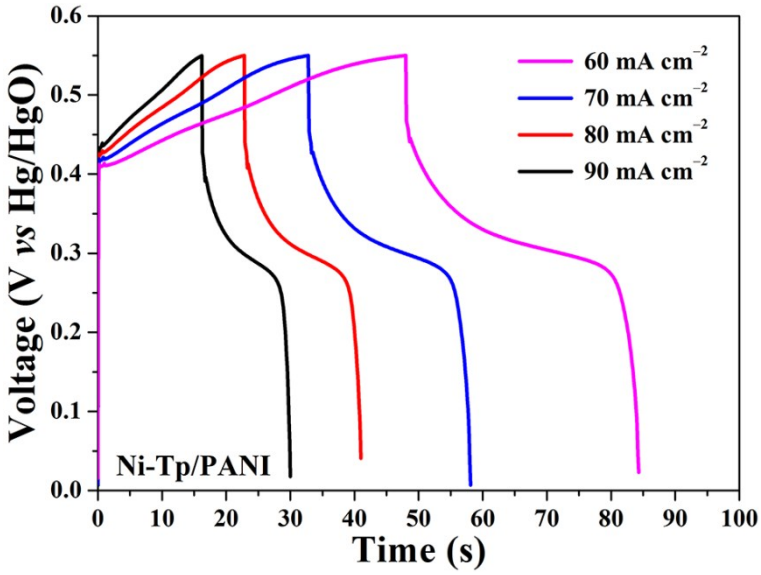

Fig. S5 GCD curves of the prepared Ni-Tp/PANI electrode at the current densities of 60, 70, 80, and 90 mA cm^{-2}.

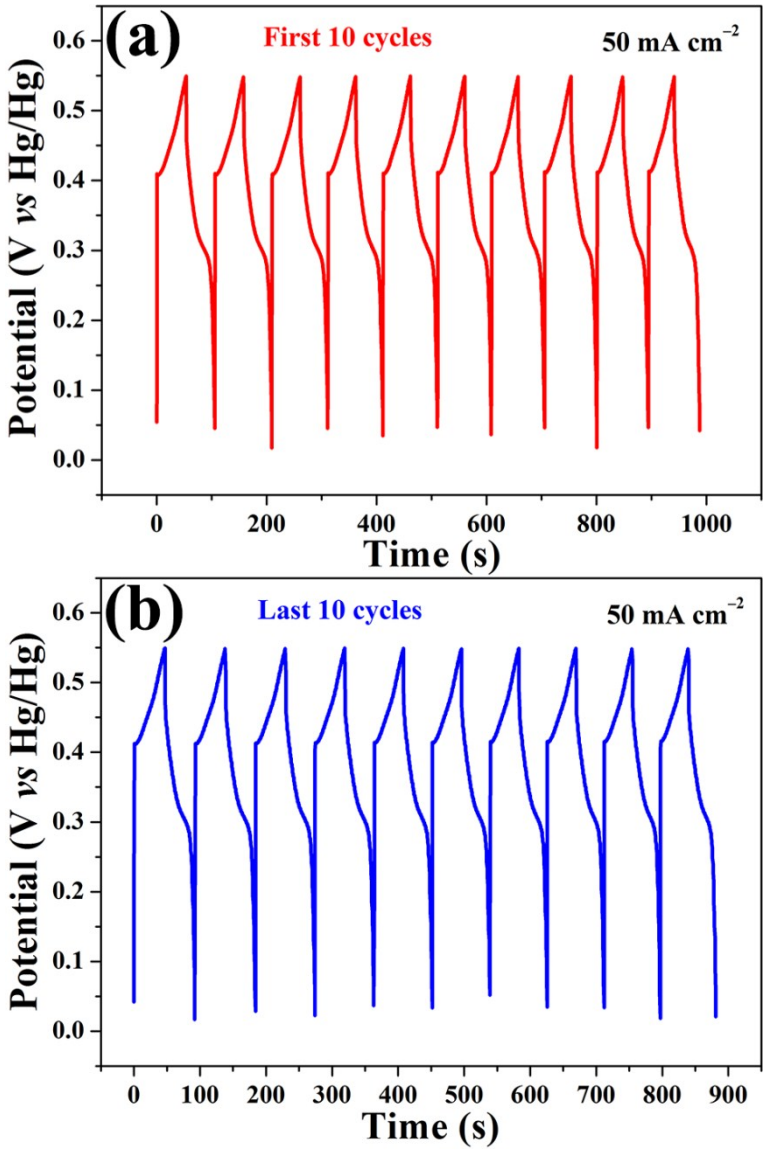

Fig. S6 The (a) first and (b) last ten charge-discharge cycles of the as-synthesized Ni-Tp/PANI electrode at a current density of 50 mA cm^{-2}.

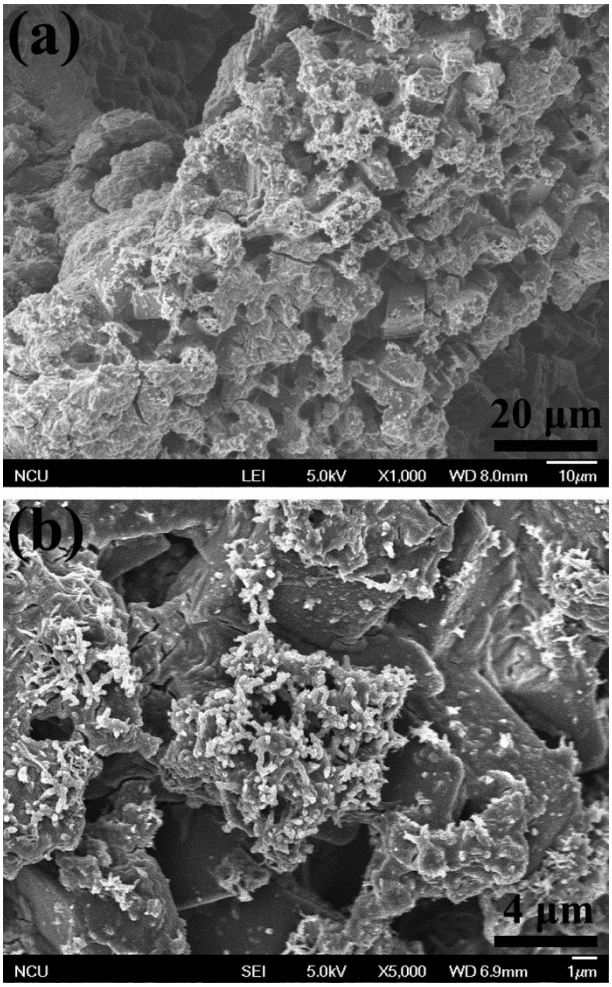

Fig. S7 (a) The low-magnification and (b) high-magnification SEM images of the Ni-Tp/PANI electrode after cycling test.

Table S1 Comparison of the electrochemical performances of the as-prepared Ni-Tp/PANI/Ni-foam with previously reported Ni-based MOF materials for supercapacitors.

Electrode	Electrolyte	Mass loading (mg cm^{-2})	C_a[a] (F cm^{-2}) (CD[c]/SR[d])	C_g[b] (F g^{-1}) (CD/SR)	ASC[e] (NE[f])	ED[g]/PD[h] (W h kg^{-1}/ W kg^{-1})	Ref.
$Ni_3(HITP)_2$	1 M $TEABF_4$/ACN	7~11	11 ×10^{-6} (1.6×10^{-4} mA cm^{-2})	70 (1 A g^{-1})	-	-	1*
Ni-imidazolate	1 M LiOH	0.1	-	306.8 (0.5 A g^{-1})	-	-	2
Ni/Co-imidazolate	1 M LiOH	0.1	-	530.4 (0.5 A g^{-1})	-	-	2
Ni-gallate/Ni-foam	6 M KOH	3	3.688 (9 mA cm^{-2})	1229.3 (3 A g^{-1})	AC	23.8/388.2 (0.5 A g^{-1})	3
Ni-DMOF-ADC	2 M KOH	1.9	-	552 (1 A g^{-1})	AC	-	4
Ni-PTA	3 M KOH	5	-	988 (1.4 A g^{-1})	AC	4.18 mW h cm^{-3}/ 231.2 mW cm^{-3} (1 mA cm^{-2})	5
Ni-salicylate	6 M KOH	20	-	1698 (1 A g^{-1})	graphene	-	6
Ni-MOF/CNT	6 M KOH	4	-	1765 (0.5 A g^{-1})	rGO/g-C_3N_4	36.6/480 (0.5 A g^{-1})	7
rGO-Ni-doped MOF	1 M KOH	-	-	758 (0.5 A g^{-1})	-	-	8
$Ni_2(DOT)$	1 M $TEABF_4$/ACN	-	0.415 (7.0×10^{-3} mA cm^{-2})	-	-	-	9*
Zn-doped Ni-BDC	6 M KOH	5	-	1620 (0.25 A g^{-1})	-	-	10
Ni-*p*-BDC	6 M KOH	5	-	1127 (0.5 A g^{-1})	-	-	11
$Ni_2CO_3(OH)_2$	6 M KOH	5.925	-	668 (5 mV s^{-1})	-	-	12
$Ni_2CO_3(OH)_2$/ZIF-8	6 M KOH	4.65	-	851 (5 mV s^{-1})	-	-	12
$Ni_3(btc)_2 \cdot 12H_2O$	2 M KOH	8	-	726 (1 A g^{-1})	AC	16.5/180[#] (0.25 A g^{-1})	13
Ni-isonicotinic	6 M KOH	3	-	634 (5 mV s^{-1})	-	-	14
Ni-Tp/PANI/Ni-foam	3 M KOH	11	10.327 (20 mA cm^{-2})	938.845 (1.818 A g^{-1})	AC	19.853/430.556 (0.556 A g^{-1})	this work

[a]C_a: areal capacitance; [b]C_g: gravimetric capacitance; [c]CD: current density; [d]SR: scan rate; [e]ASC: asymmetric supercapacitor; [f]NE: negative electrode; [g]ED: energy density; [h]PD: power density; *Note: electrochemical performances were measured in a two-electrode configuration, others in three-electrode configuration. The areal capacitance, together with the current density, was normalized to specific surface area (630 m^2 g^{-1}) for Ref. 1, and to stack volume (7.9×10^{-3} cm^3) for Ref. 9; [#]The power density value was obtained by estimation which was not provided in the text.

Table S2 Comparison of the electrochemical performances of the as-prepared Ni-Tp/PANI with previously reported Ni-based compounds directly grown on Ni foam for supercapacitors.

Electrode	Electrolyte	Mass loading (mg cm^{-2})	C_a[a] (F cm^{-2}) (CD[c]/SR[d])	C_g[b] (F g^{-1}) (CD/SR)	ASC[e] (NE[f])	ED[g]/PD[h] (W h kg^{-1}/ W kg^{-1})	Ref.
$Ni(OH)_2$ nanosheets	2 M KOH	2	4.8 (2 mA cm^{-2})	2384.3 (1 A g^{-1})	-	-	15
$Ni(OH)_2$ platelets	2 M KOH	3	0.43 (1 A g^{-1})	1422 (1 A g^{-1})	-	-	16
Ni-Co LDH	1 M KOH	3	1.6 (1.8 mA cm^{-2})	2682 (3 A g^{-1})	rGO	188/1499 (1 A g^{-1})	17
$Ni(OH)_2$/CNT	6 M KOH	4.85	16 (2.5 mA cm^{-2})	3300 (0.5 A g^{-1})	AC	50.6/95 (2.5 mA cm^{-2})	18
NiO nanosheets	2 M KOH	0.15	0.376 (13.4 A g^{-1})	2504.3 (13.4 A g^{-1})	-	-	19
NiO Nanorod Arrays	1 M NaOH	2.2	4.44 (5 mA cm^{-2})	2018 (2.27 A g^{-1})	-	-	20
$Ni_xCo_{3-x}O_4$ nanowires	2 M KOH	2.5	3.7 (2.5 mA cm^{-2})	1479 (1 A g^{-1})	AC	37.4/163 (3.6 mA cm^{-2})	21
$Cu_{0.2}Ni_{0.8}O$ nanowires	1 M KOH	4	2.24 (2.5 mA cm^{-2})	1955 (1 mV s^{-1})	AC	29.7/129 (2 mA cm^{-2})	22
$NiCo_2O_4$ nanoneedles	2 M KOH	0.9	1.01 (5.56 mA cm^{-2})	1118.6 (5.56 mA cm^{-2})	-	-	23
$NiCo_2O_4$ nanosheets1	2 M KOH	1.2	3.51 (1.8 mA cm^{-2})	2925 (1.5 A g^{-1})	-	-	24
$NiCo_2O_4$ nanosheets2	3 M KOH	0.8	1.61 (1.6 mA cm^{-2})	2010 (2 A g^{-1})	-	-	25
$NiCo_2O_4$ nanowires	3 M KOH	3	8.04 (2 A g^{-1})	2681 (2 A g^{-1})	-	-	26
$NiCo_2O_4$@ $NiCo_2O_4$	2 M KOH	1.97	1.55 (2 mA cm^{-2})	787 (2 mA cm^{-2})	-	-	27
$NiMoO_4$ nanosheets	2 M KOH	1.2	1.47 (1 A g^{-1})	1221.2 (1 A g^{-1})	AC	60.9/850 (1 A g^{-1})	28
$NiMoO_4$ nanowires	2 M KOH	1.5	4.94 (8 mA cm^{-2})	3293 (5.3 A g^{-1})	-	-	29
$NiWO_4$ nanostructure	2 M KOH	0.75	0.6 (1 A g^{-1})	797.8 (1 A g^{-1})	-	-	30
$NiMn_2O_4$ nanosheets	6 M KOH	0.17	0.11 (1 A g^{-1})	662.5 (1 A g^{-1})	-	-	31
$NH_4NiPO_4 \cdot H_2O$	3 M KOH	1~1.5 mg	-	1513 (5 A g^{-1})	AC	41.6/375 (0.5 A g^{-1})	32
$NiCo_2O_4$@$NiWO_4$	6 M KOH	3.66	5.07 (1 A g^{-1})	1384 (1 A g^{-1})	AC	41.5/760 (1 A g^{-1})	33
$NiCo_2O_4$@Ni_3S_2	2 M KOH	2.1	3.6 (1 A g^{-1})	1716 (1 A g^{-1})	-	-	34
Ni_3S_2 nanosheets	6 M KOH	2	2.74 (2 A g^{-1})	1370.4 (2 A g^{-1})	AC	34.6/150.4 (0.2 A g^{-1})	35
NiS_2 hollow prisms	2 M LiOH	1	1.73 (5 A g^{-1})	1725 (5 A g^{-1})	-	-	36
Ni_3S_2@β-NiS	6 M KOH	-	-	1158 (2 A g^{-1})	AC	55.1/925.9 (1 A g^{-1})	37
Ni_3S_2@MoS_2	2 M KOH	-	-	848 (5 A g^{-1})	-	-	38
Ni-Co sulfide	1 M KOH	2.5	6 (2.5 mA cm^{-2})	2415 (1 A g^{-1})	AC	25/447 (8 mA cm^{-2})	39
$NiCo_2S_4$ core-shell	6 M KOH	1	1.948 (1 mA cm^{-2})	1948 (1 A g^{-1})	Porous C	22.8/160 (1 mA cm^{-2})	40
$NiCo_2S_4$ nanotubes1	6 M KOH	4.2	3.3 (2 A g^{-1})	783 (2 A g^{-1})	-	-	41
$NiCo_2S_4$ nanotubes2	6 M KOH	6	14.39 (5 mA cm^{-2})	2398 (5 mA cm^{-2})	rGO	31.5/156.6 (10 mA cm^{-2})	42
$CoNi_2S_4$ mushroom	2 M KOH	2.1	5.82 (10 mA cm^{-2})	2700 (4.76 A g^{-1})	-	-	43
$CoNi_2S_4$ nanosheets	2 M KOH	2.2	6.39 (5 mA cm^{-2})	2906 (2.27 A g^{-1})	AC	33.9/409 (10 mA cm^{-2})	44
Ni_2P nanosheets	6 M KOH	1.2	4.2 (3 mA cm^{-2})	3496 (2.5 A g^{-1})	AC	26/337 (5 mV s^{-1})	45
Ni-Tp/PANI/Ni-foam	3 M KOH	11	10.327 (20 mA cm^{-2})	938.845 (1.818 A g^{-1})	AC	19.853/430.556 (0.556 A g^{-1})	this work

[a]C_a: areal capacitance; [b]C_g: gravimetric capacitance; [c]CD: current density; [d]SR: scan rate; [e]ASC: asymmetric supercapacitor; [f]NE: negative electrode; [g]ED: energy density; [h]PD: power density.

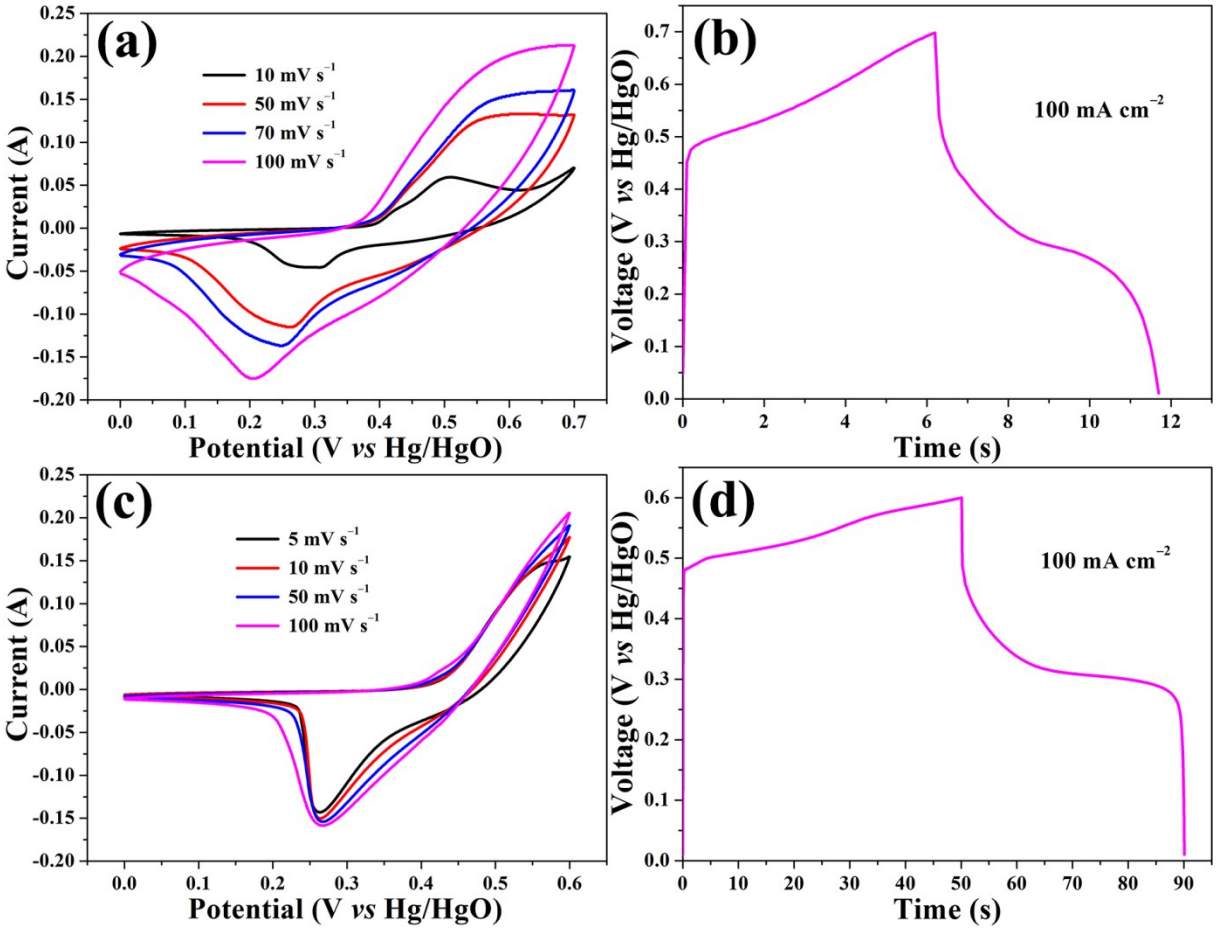

Fig. S8 (a) CV curves of the Ni-Tp/PANI electrode at different scan rates in 3 M KOH aqueous solution in the potential window of 0–0.7 V (vs. Hg/HgO). (b) GCD curve of the Ni-Tp/PANI electrode at the current density of 100 mA cm^{-2} in the potential window of 0–0.7 V (vs. Hg/HgO). (c) CV curves of the Ni-Tp electrode at different scan rates in 3 M KOH aqueous solution in the potential window of 0–0.6 V (vs. Hg/HgO). (d) GCD curve of the Ni-Tp electrode at the current density of 100 mA cm^{-2} in the potential window of 0–0.6 V (vs. Hg/HgO).

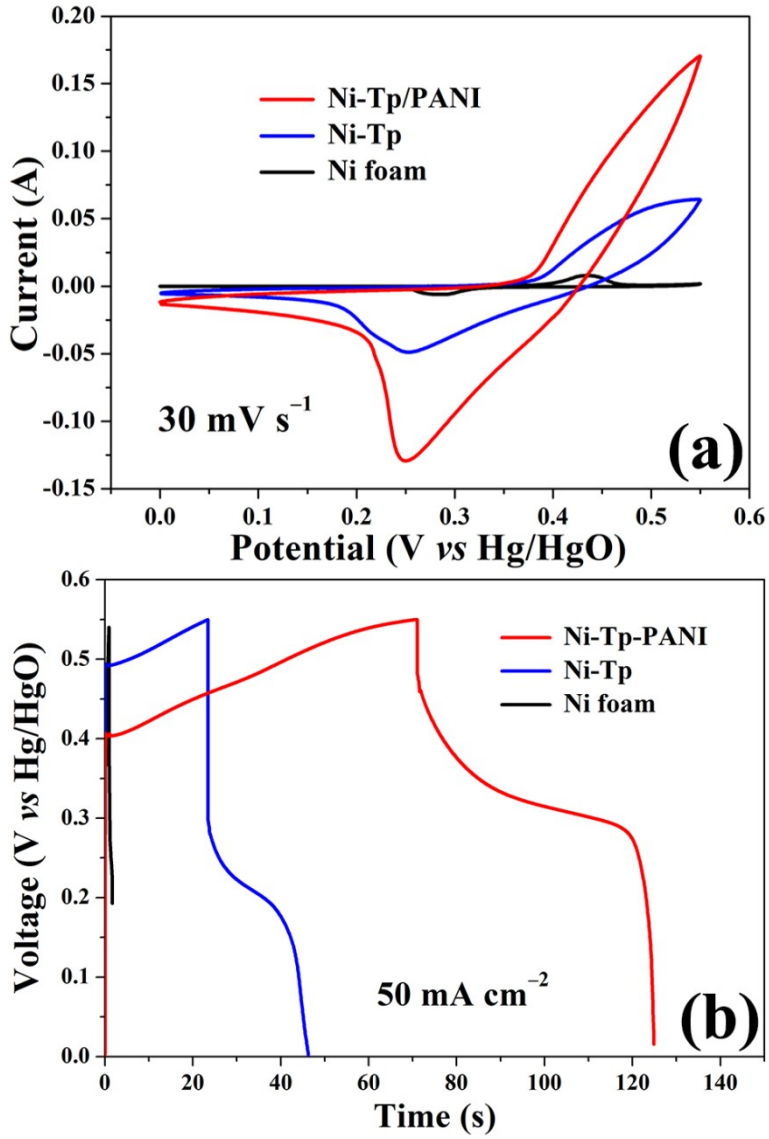

Fig. S9 (a) Comparison of CV curves of the as-prepared Ni-Tp and Ni-Tp/PANI electrodes and the bare Ni foam at a scan rate of 30 mV s^{-1}. (b) Comparison of GCD curves of the as-prepared Ni-Tp and Ni-Tp/PANI electrodes and the bare Ni foam at a current density of 50 mA cm^{-2}.

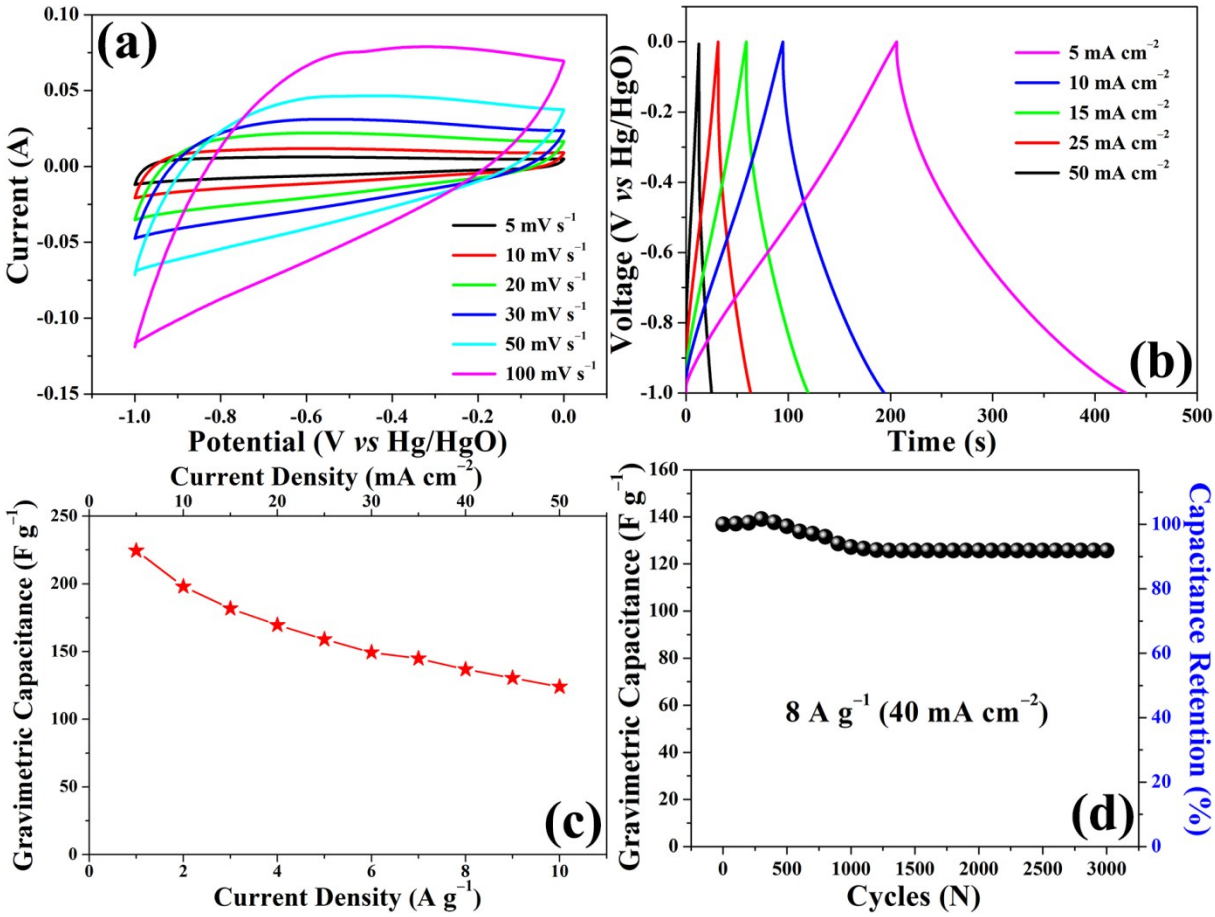

Fig. S10 (a) CV curves of the activated carbon electrode at different scan rates in 3 M KOH aqueous solution. (b) GCD curves of the activated carbon electrode at different current densities. (c) The gravimetric capacitance of the activated carbon electrode as a function of current density. (d) Cycling performance of the activated carbon electrode at a current density of 8 A g^{-1} (40 mA cm^{-2}) in 3 M KOH aqueous solution.

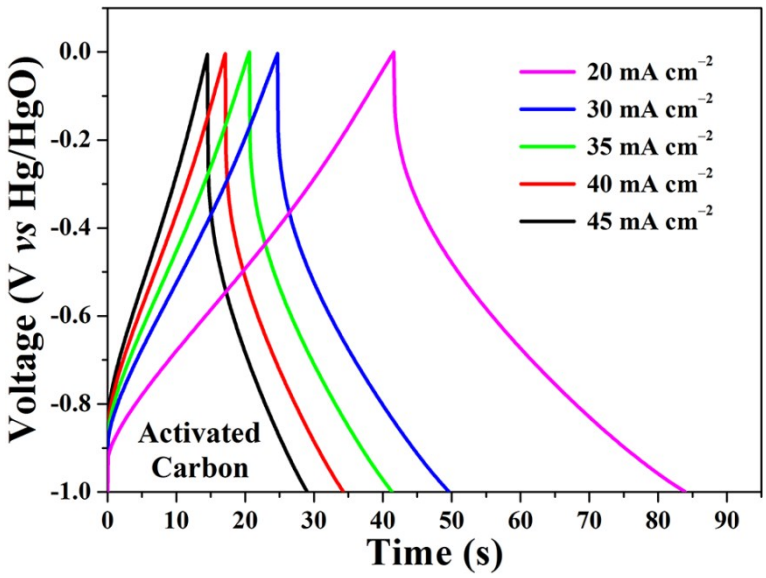

Fig. S11 GCD curves of the prepared activated carbon electrode at the current densities of 20, 30, 35, 40, and 45 mA cm^{-2}.

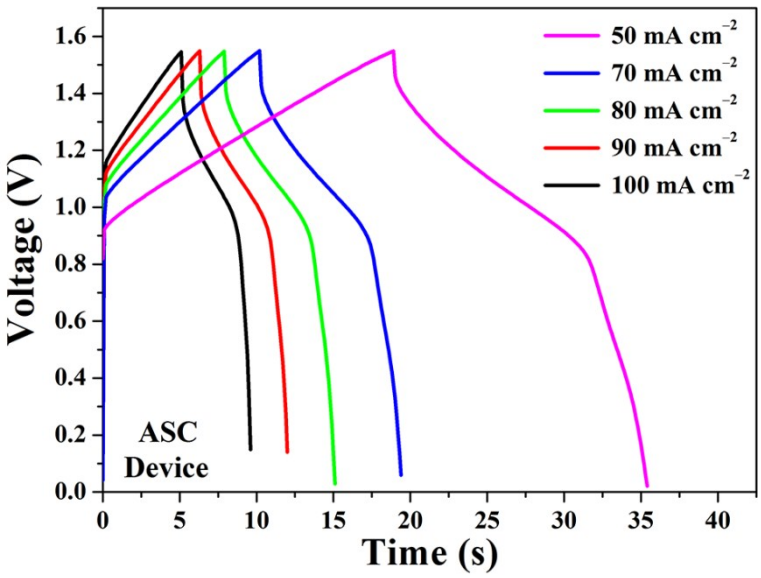

Fig. S12 GCD curves of the assembled ASC device at the current densities of 50, 70, 80, 90, and 100 mA cm^{-2}.

References

1 D. Sheberla, J. C. Bachman, J. S. Elias, C. J. Sun, Y. Shao-Horn and M. Dincă, Conductive MOF electrodes for stable supercapacitors with high areal capacitance, *Nat. Mater.*, 2017, **16**, 220–224.

2 H. C. Xia, J. N. Zhang, Z. Yang, S. Y. Guo, S. H. Guo and Q. Xu, 2D MOF nanoflake-assembled spherical microstructures for enhanced supercapacitor and electrocatalysis performances, *Nano-Micro Lett.*, 2017, **9**, 43.

3 Q. L. Chen, S. J. Lei, L. F. Chen, P. Q. Deng, Y. H. Xiao and B. C. Cheng, A novel fluffy nanostructured 3D network of $Ni(C_7H_4O_5)$ for supercapacitors, *Electrochim. Acta*, 2017, **230**, 141–150.

4 C. Qu, Y. Jiao, B. Zhao, D. C. Chen, R. Q. Zou, K. S. Walton and M. L. Liu, Nickel-based pillared MOFs for high-performance supercapacitors: Design, synthesis and stability study, *Nano Energy*, 2016, **26**, 66–73.

5 Y. Yan, P. Gu, S. S. Zheng, M. B. Zheng, H. Pang and H. G. Xue, Facile synthesis of an accordion-like Ni-MOF superstructure for high-performance flexible supercapacitors, *J. Mater. Chem. A*, 2016, **4**, 19078–19085.

6 J. Xu, C. Yang, Y. F. Xue, C. Wang, J. Y. Cao and Z. D. Chen, Facile synthesis of novel metal-organic nickel hydroxide nanorods for high performance supercapacitor, *Electrochim. Acta*, 2016, **211**, 595–602.

7 P. Wen, P. W. Gong, J. F. Sun, J. Q. Wang and S. R. Yang, Design and synthesis of Ni-MOF/CNT composites and rGO/carbon nitride composites for an asymmetric supercapacitor with high energy and power density, *J. Mater. Chem. A*, 2015, **3**, 13874–13883.

8 P. C. Banerjee, D. E. Lobo, R. Middag, W. K. Ng, M. E. Shaibani and M. Majumder, Electrochemical capacitance of Ni-doped metal organic framework and reduced graphene oxide composites: More than the sum of its parts, *ACS Appl. Mater. Interfaces*, 2015, **7**, 3655−3664.

9 K. M. Choi, H. M. Jeong, J. H. Park, Y. B. Zhang, J. K. Kang and O. M. Yaghi, Supercapacitors of nanocrystalline metal organic frameworks, *ACS Nano*, 2014, **8**, 7451–7457.

10 J. Yang, C. Zheng, P. X. Xiong, Y. F. Li and M. D. Wei, Zn-doped Ni-MOF material with a high supercapacitive performance, *J. Mater. Chem. A*, 2014, **2**, 19005–19010.

11 J. Yang, P. X. Xiong, C. Zheng, H. Y. Qiu and M. D Wei, Metal–organic frameworks: A new promising class of materials for a high performance supercapacitor electrode, *J. Mater. Chem. A*, 2014, **2**, 16640–16644.

12 Y. L. Gao, J. X. Wu, W. Zhang, Y. Y. Tan, J. Gao, B. H. J. Tang and J. C. Zhao, Synthesis of nickel carbonate hydroxide/zeolitic imidazolate framework-8 as a supercapacitors electrode, *RSC Adv.*, 2014, **4**, 36366–36371.

13 L. Kang, S. X. Sun, L. B. Kong, J. W. Lang and Y. C. Luo, Investigating metal-organic framework as a new pseudo-capacitive material for supercapacitors, *Chin. Chem. Lett.*, 2014, **25**, 957–961.

14 C. M Liao, Y. K. Zuo, W. Zhang, J. C. Zhao, B. H. J. Tang, A. M. Tang, Y. H. Sun and J. L. Xu, Electrochemical performance of metal-organic framework synthesized by a solvothermal method for supercapacitors, *Russ. J. Electrochem.*, 2013, **49**, 983–986.

15 X. H. Xiong, D. Ding, D. C. Chen, G. Waller, Y. F. Bu, Z. X. Wang and M. L. Liu, Three-dimensional ultrathin $Ni(OH)_2$ nanosheets grown on nickel foam for high-performance supercapacitors, *Nano Energy*, 2015, **11**, 154–161.

16 L. J. Li, J. Xu, J. L. Lei, J. Zhang, F. McLarnon, Z. D. Wei, N. B. Li and F. S. Pan, A one-step,

cost-effective green method to in situ fabricate $Ni(OH)_2$ hexagonal platelets on Ni foam as binder-free supercapacitor electrode materials, *J. Mater. Chem. A*, 2015, **3**, 1953–1960.

17 H. Chen, L. F. Hu, M. Chen, Y. Yan and L. M. Wu, Nickel-cobalt layered double hydroxide nanosheets for high-performance supercapacitor electrode materials, *Adv. Funct. Mater.*, 2014, **24**, 934–942.

18 Z. Tang, C. H. Tang and H. Gong, A high energy density asymmetric supercapacitor from nano-architectured $Ni(OH)_2$/carbon nanotube electrodes, *Adv. Funct. Mater.*, 2012, **22**, 1272–1278.

19 G. H. Cheng, W. F. Yang, C. Q. Dong, T. Y. Kou, Q. G. Bai, H. Wang and Z. H. Zhang, Ultrathin mesoporous NiO nanosheet-anchored 3D nickel foam as an advanced electrode for supercapacitors, *J. Mater. Chem. A*, 2015, **3**, 17469–17478.

20 Z. Y. Lu, Z. Chang, J. F. Liu and X. M. Sun, Stable ultrahigh specific capacitance of NiO nanorod arrays, *Nano Res.*, 2011, **4**, 658–665.

21 X. Wang, C. Y. Yan, A. Sumboja and P. S. Lee, High performance porous nickel cobalt oxide nanowires for asymmetric supercapacitor, *Nano Energy*, 2014, **3**, 119–126.

22 L. Y. Zhang, C. H. Tang and H. Gong, Temperature effect on the binder-free nickel copper oxide nanowires with superior supercapacitor performance, *Nanoscale*, 2014, **6**, 12981–12989.

23 G. Q. Zhang, H. B. Wu, H. E. Hoster, M. B. Chan-Park and X. W. Lou, Single-crystalline $NiCo_2O_4$ nanoneedle arrays grown on conductive substrates as binder-free electrodes for high-performance supercapacitors, *Energy Environ. Sci.*, 2012, **5**, 9453–9456.

24 G. Q. Zhang and X. W. Lou, General solution growth of mesoporous $NiCo_2O_4$ nanosheets on various conductive substrates as high-performance electrodes for supercapacitors, *Adv. Mater.*, 2013, **25**, 976–979.

25 C. Z. Yuan, J. Y. Li, L. R. Hou, X. G. Zhang, L. F. Shen and X. W. Lou, Ultrathin mesoporous $NiCo_2O_4$ nanosheets supported on Ni foam as advanced electrodes for supercapacitors, *Adv. Funct. Mater.*, 2012, **22**, 4592–4597.

26 Q. F. Wang, X. F. Wang, B. Liu, G. Yu, X. J. Hou, D. Chen and G. Z. Shen, $NiCo_2O_4$ nanowire arrays supported on Ni foam for high-performance flexible all-solid-state supercapacitors, *J. Mater. Chem. A*, 2013, **1**, 2468–2473.

27 X. Y. Liu, S. J. Shi, Q. Q. Xiong, L. Li, Y. J. Zhang, H. Tang, C. D. Gu, X. L. Wang and J. P. Tu, Hierarchical $NiCo_2O_4$@$NiCo_2O_4$ core/shell nanoflake arrays as high-performance supercapacitor materials, *ACS Appl. Mater. Interfaces*, 2013, **5**, 8790−8795.

28 S. J. Peng, L. L. Li, H. B. Wu, S. Madhavi and X. W. Lou, Controlled growth of $NiMoO_4$ nanosheet and nanorod arrays on various conductive substrates as advanced electrodes for asymmetric supercapacitors, *Adv. Energy Mater.*, 2015, **5**, 1401172.

29 D. Guo, P. Zhang, H. M. Zhang, X. Z. Yu, J. Zhu, Q. H. Li and T. H. Wang, $NiMoO_4$ nanowires supported on Ni foam as novel advanced electrodes for supercapacitors, *J. Mater. Chem. A*, 2013, **1**, 9024–9027.

30 G. J. He, J. M. Li, W. Y. Li, B. Li, N. Noor, K. B. Xu, J. Q. Hu and I. P. Parkin, One pot synthesis of nickel foam supported self-assembly of $NiWO_4$ and $CoWO_4$ nanostructures that act as high performance electrochemical capacitor electrodes, *J. Mater. Chem. A*, 2015, **3**, 14272–14278.

31 H. M. Wei, J. X. Wang, L. Yu, Y. Y. Zhang, D. W. Hou and T. F. Li, Facile synthesis of $NiMn_2O_4$ nanosheet arrays grown on nickel foam as novel electrode materials for high-performance supercapacitors, *Ceram. Int.*, 2016, **42**, 14963–14969.

32 C. Chen, N. Zhang, X. H. Liu, Y. L. He, H. Wan, B. Liang, R. Z. Ma, A. Q. Pan and V. A. L. Roy, Polypyrrole-modified $NH_4NiPO_4·H_2O$ nanoplate arrays on Ni foam for efficient electrode in electrochemical capacitors, *ACS Sustainable Chem. Eng.*, 2016, **4**, 5578−5584.

33 S. M. Chen, G. Yang, Y. Jia and H. J. Zheng, Three-dimensional $NiCo_2O_4$@$NiWO_4$ core–shell nanowire arrays for high performance supercapacitors, *J. Mater. Chem. A*, 2017, **5**, 1028–1034.

34 J. P. Wang, S. L. Wang, Z. C. Huang and Y. M. Yu, High-performance $NiCo_2O_4$@Ni_3S_2 core/shell mesoporous nanothorn arrays on Ni foam for supercapacitors, *J. Mater. Chem. A*, 2014, **2**, 17595–17601.

35 H. H. Huo, Y. Q. Zhao and C. L. Xu, 3D Ni_3S_2 nanosheet arrays supported on Ni foam for high-performance supercapacitor and non-enzymatic glucose detection, *J. Mater. Chem. A*, 2014, **2**, 15111–15117.

36 Z. Y. Dai, X. X. Zang, J. Yang, C. C. Sun, W. L. Si, W. Huang and X. C. Dong, Template synthesis of shape-tailorable NiS_2 hollow prisms as high-performance supercapacitor materials, *ACS Appl. Mater. Interfaces*, 2015, **7**, 25396−25401.

37 W. Li, S. L. Wang, L. P. Xin, M. Wu and X. J. Lou, Single-crystal β-NiS nanorod arrays with a hollow-structured Ni_3S_2 framework for supercapacitor applications, *J. Mater. Chem. A*, 2016, **4**, 7700–7709.

38 J. Wang, D. L. Chao, J. L. Liu, L. L. Li, L. F. Lai, J. Y. Lin and Z. X. Shen, Ni_3S_2@MoS_2 core/shell nanorod arrays on Ni foam for high-performance electrochemical energy storage, *Nano Energy*, 2014, **7**, 151–160.

39 Y. H. Li, L. J. Cao, L. Qiao, M. Zhou, Y. Yang, P. Xiao and Y. H. Zhang, Ni–Co sulfide nanowires on nickel foam with ultrahigh capacitance for asymmetric supercapacitors, *J. Mater. Chem. A*, 2014, **2**, 6540–6548.

40 W. Kong, C. C. Lu, W. Zhang, J. Pu and Z. H. Wang, Homogeneous core–shell $NiCo_2S_4$ nanostructures supported on nickel foam for supercapacitors, *J. Mater. Chem. A*, 2015, **3**, 12452–12460.

41 J. Pu, T. T. Wang, H. Y. Wang, Y. Tong, C. C. Lu, W. Kong and Z. H. Wang, Direct growth of $NiCo_2S_4$ nanotube arrays on nickel foam as high-performance binder-free electrodes for supercapacitors, *ChemPlusChem*, 2014, **79**, 577–583.

42 H. C. Chen, J. J. Jiang, L. Zhang, D. D. Xia, Y. D. Zhao, D. Q. Guo, T. Qi and H. Z. Wan, *In situ* growth of $NiCo_2S_4$ nanotube arrays on Ni foam for supercapacitors: Maximizing utilization efficiency at high mass loading to achieve ultrahigh areal pseudocapacitance, *J. Power Sources*, 2014, **254**, 249–257.

43 L. Mei, T. Yang, C. Xu, M. Zhang, L. B. Chen, Q. H. Li and T. H. Wang, Hierarchical mushroom-like $CoNi_2S_4$ arrays as a novel electrode material for supercapacitors, *Nano Energy*, 2014, **3**, 36–45.

44 W. Hu, R. Q. Chen, W. Xie, L. L. Zou, N. Qin and D. H. Bao, $CoNi_2S_4$ nanosheet arrays supported on nickel foams with ultrahigh capacitance for aqueous asymmetric supercapacitor applications, *ACS Appl. Mater. Interfaces*, 2014, **6**, 19318−19326.

45 K. Zhou, W. J. Zhou, L. J. Yang, J. Lu, S. Cheng, W. J. Mai, Z. H. Tang, L. G. Li and S. W. Chen, Ultrahigh-performance pseudocapacitor electrodes based on transition metal phosphide nanosheets array via phosphorization: A general and effective approach, *Adv. Funct. Mater.*, 2015, **25**, 7530–7538.